

**REVIEW OF AERONAUTICAL FATIGUE
INVESTIGATIONS IN JAPAN
DURING THE PERIOD JUNE 2019 TO MAY 2021**

Edited by

Shigeru Machida

Takao Okada

Japan Aerospace Exploration Agency

The ICAF 2021 website

The International Committee on Aeronautical Fatigue and Structural Integrity

CONTENTS

	page
<u>1. INTRODUCTION</u>	1
<u>2. FATIGUE AND FAILURE IN METALLIC MATERIALS AND COMPONENTS</u>	
2.1 Build Direction Effect on the Fatigue Properties of Electron Beam Melted Ti-6Al-4V	4
<u>3. FATIGUE AND FAILURE IN COMPOSITE MATERIALS AND COMPONENTS</u>	
3.1 Effect of Interface Nanostructure on Fatigue Delamination Growth of CFRTP and Aluminum Alloy Jointed by Direct Thermal Welding	7
3.2 Improving Damage Tolerance of Composite T-joints Using Interlocking-Fiber-Based Crack Arresters	9
3.3 Galvanic Corrosion Testing Procedures for CFRP-Metal Assemblies	12
3.4 Design and Manufacturing Trial of a Biomimetic Structure Based on Topology Optimization	14
<u>4. STRUCTURAL HEALTH MONITORING</u>	
4.1 Flight Demonstration Test for Optical Fiber Sensor based Impact Damage Detection System	18
<u>5. MISCELLANEOUS</u>	
5.1 Smart Wing Load Alleviation Through Optical Fiber Sensing, Load Identification, and Deep Reinforcement Learning	21

5.2 Scarf Sanding Technology for Carbon Fiber Reinforced Plastics (CFRP) Airframe	24
5.3 Thermography measurement for specimen with non-uniform emissivity surface	27
5.4 Aircraft Accident and Serious Incident Investigation	29
<u>ACKNOWLEDGEMENTS</u>	32

1. INTRODUCTION

Shigeru Machida, Chairperson of the Special Committee for ICAF in The Japan Society of Aeronautical and Space Sciences

This review summarizes the papers on the study of aeronautical fatigue, structural integrity and related themes conducted in Japan during June 2019 to May 2021.

The papers were contributed by following organizations:

Acquisition, Technology & Logistics Agency (ATLA)

Japanese Civil Aviation Bureau (JCAB)

Japan Transport Safety Board (JTSB)

Japan Aircraft Development Corporation (JADC)

The Society of Japanese Aerospace Companies (SJAC)

Mitsubishi Heavy Industries, Ltd. (MHI)

Mitsubishi Aircraft Corporation

Kawasaki Heavy Industries, Ltd. (KHI)

SUBARU CORPORATION

IHI Corporations

ShinMaywa Industries, Ltd.

NIPPI Corporation

Sumitomo Precision Products Co., Ltd.

JAMCO Corporation

JAL Engineering Co., Ltd.

All Nippon Airways Co., Ltd.

The University of Tokyo

Nagaoka University of Technology

Waseda University

Tokyo University of Science

Kanagawa Institute of Industrial Science and Technology

Japan Aerospace Exploration Agency (JAXA)

The second half of the period April 2019 - April 2021, we found the abrupt change of economic situation and ways of our life due to the COVID-19 pandemic and still we are. Air transportation world is impacted by the spread of the COVID-19 pandemic as well. Based on Statistic data from Ministry of Land, Infrastructure, Transport and Tourism, number of air travel passenger by Japanese Airlines in 2020 was 7% for domestic and 2% for international of May, 2019, and 45% for domestic and 6% for

international of December, 2019. Impact of the COVID-19 is continuing on international air transportation strongly. Our activities on industries, R&D institutes and academies are also impacted and ways of communication should be changed due to the COVID-19 crisis.

The general activities on aircraft development program in Japan during 2019 to 2021 is summarized as follows:

- The development of Mitsubishi SpaceJet, which was Mitsubishi Regional Jet, (MRJ) previously, is in the final stage and various steps for the certification is being made. The first flight was successfully completed in November 2015. The production is underway at Mitsubishi Aircraft Corporation in Nagoya. Certification flight testing started in January 2019 at Moses Lake in U.S.A. In March 2020, it has completed the maiden flight of Flight Test Vehicle 10 (FTV10), the first Mitsubishi SpaceJet M90 in final, certifiable baseline configuration. The FTV10 took off from the Prefectural Nagoya Airport and basic performance tests were conducted over the Pacific Ocean.
- Mitsubishi Heavy Industries, Ltd. (MHI), Kawasaki Heavy Industries, Ltd. (KHI), Subaru Corporation, ShinMaywa Industries, Ltd. (SMIC) and NIPPI Corporation (NIPPI) have been participating in the project to develop and produce The Boeing Company's next-generation large-size passenger jet, the Boeing 777X. The first flight was conducted over Washington state in January 2020.
- Japanese companies are playing an important role in the international joint development and taking part as the manufacture of the low pressure turbine components of GE9X engines for Boeing777X. In September 2020, this engine has been certified by the U.S. aviation safety regulator.
- Japanese companies are developing advanced technologies for electrified aircraft system, such as engine-embedded electric machine and air-cooling system for aircraft onboard 100kW-class power electronics, to contribute to mitigation of climate change through total energy management of aircraft.
- The Japan-led F-X development program, which will succeed to the Japan Air Self-Defense Force (JASDF) F-2 fighter jet, has started in 2020.
- “Structural Materials for Innovation” (SM⁴I) Project started in 2014 as a part of SIP (Cross-ministerial Strategic Innovation Promotion Program) supported by the Council for Science, Technology and Innovation (CSTI) of the Cabinet Office, Japan. New material development is underway. The first phase of SIP ended in 2018 being followed by the second phase. From the material development point of view, its purpose is to develop a next-generation Materials Integration (MI) system for the inverse design creating desired performance, materials and process,

leading the world utilizing the technical foundation of MI being developed so far. Following three domains construct the research project: A: Establishment of Inverse Design MI Basis for Advanced Structural Materials and Processes, B: Application of the Inverse Design MI to Actual Structural Materials (CFRP), and C: Application of the Inverse Design MI to Actual Structural Materials (3D Powder Processing). For establishment of the inverse design MI basis, multi-physics/multi-scale simulator will be developed and multifunctional composite material or adaptive structural element using composite material be proposed. The research and development of multi-ingredient network polymers, structural design using the developed polymers, and its manufacturing are calculated using the simulator. Comparing to the conventional hand layup, accuracy of layup using (Automated Fiber Placement) equipment is degraded and it aggregates mechanical properties such as rigidity, strength and etc. For application of the inverse design MI, the improvement of the quality caused by AFP is achieved the application of multi-physics/multi-scale simulation and MI. Currently, the panel with stress concentration is manufactured and technical issues have been identified.

- The WEATHER (Weather Endurance Aircraft Technology to Hold, Evade and Recover) -Eye consortium was established in 2016, in order to improve the operational safety and efficiency under the severe weather condition. A slippery short runway in winter, aircraft lightning potential detection, lightning resistant composite material, lightning attachment prevention, detection of crystal ice drop and volcanic ash, prevention of fan blade icing, deposition prevention and erosion protection of the turbine blade were selected for research topic. In 2021, 23 organizations join as steering organization and 16 organizations join as partner organization. From the material point of view, development of the CFRP with high conductivity through the thickness direction using conductive polymer have been conducted to reduce the lightning damage. High conductive polymer was developed and the reduction of the lightning damage using the polymer was demonstrated.

2 FATIGUE AND FAILURE IN METALLIC MATERIALS AND COMPONENTS

2.1 Build direction effect on the fatigue properties of electron beam melted Ti-6Al-4V

Hiroshi Nakamura^{1*}, Masashi Mori², Yoshihiko Nagata²

¹ IHI Corporation, Aero-Engine & Space Operations, Kanagawa, Japan

² IHI Corporation, Technology & Intelligence Integration, Kanagawa, Japan

Additive manufacturing (AM) technology has a great potential to be used as aero engine components. This is because that AM could produce parts or shapes with near-net or final geometry, including complex feature, and reduce structural weight. The approach to build a part by adding material layer by layer using structural metal alloys represents a significantly different approach than conventional wrought or cast processes. The resulting material and its properties may differ from that produced conventional process such as microstructure, defect species, structural strength and durability. The requirement for design, structural assessment is required to ensure safety of AM parts. Anisotropic strength is one of the issues to use AM material as aero engine component parts. Several studies have been reported the fatigue test results of AM materials, however, investigation regarding the effect of build direction on fatigue properties of AM Ti-6Al-4V is still insufficient. This work focuses on the effect of build direction on the fatigue properties of electron beam melted (EBM) Ti-6Al-4V. Three kind of specimens were manufactured in different build directions as 0°, 45°, and 90°. An electron beam machine, ArcamQ20+ was used to fabricate the AM bulk specimens. HIP and annealing were carried out as post-processing. The specimens were machined to finish the surface. Fatigue tests were conducted using smooth bar specimen at ambient air and room temperature. Crack growth tests were carried out using CT specimen. Fracture surfaces were observed after the fatigue tests.

S-N diagram of EBM Ti-6Al-4V is shown in Figure 2.1-1. This figure includes S-N curves of Ti-6Al-4V wrought and casting which were referred from literature (*1). Low cycle and high cycle fatigue lives of all EBM Ti-6Al-4V specimens were almost same as that of the wrought. Middle cycle fatigue lives in build direction of 0° and 90° were shorter than that of the wrought, however they were still longer than that of the casting. Only specimen in build direction of 45° in middle cycle showed similar fatigue life to that of the wrought. Figures 2.1-2 show typical fatigue origins. Specimens of all EBM Ti-6Al-4V in low cycle lives have surface fatigue origin. Metallurgical flat surface can be seen in fatigue origin (Figure 2.1-2 (a)). High cycle and middle cycle fatigue lives of the EBM have both surface fatigue origin and that of interior. Incompletely melted particles, micro cracks can be seen in interior fatigue origin (Figure 2.1-2 (b)). Relationship between crack length and cycles of EBM Ti-6Al-4V with different build direction is shown in Figure 2.1-3. The specimens in build direction of 45° indicate better crack growth resistance than those of the others build

directions.

Shorter fatigue lives in build direction of 0° and 90° than that of the wrought may attribute to distribution of fatigue origin size and location. Build direction can also affect the fatigue crack growth life. Better crack growth resistance in build direction of 45° may result in similar fatigue lives to that of the wrought, and smaller scatter of fatigue lives than those of the others build direction.

*1) Battelle Memorial Institute, MMPDS-09

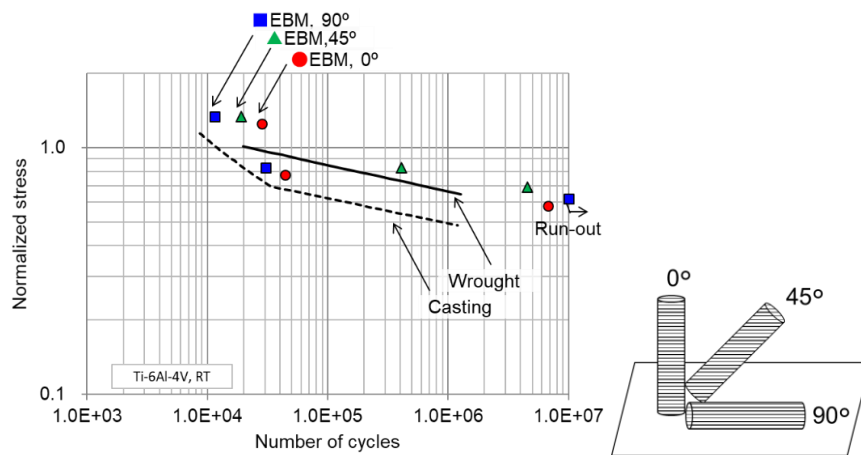
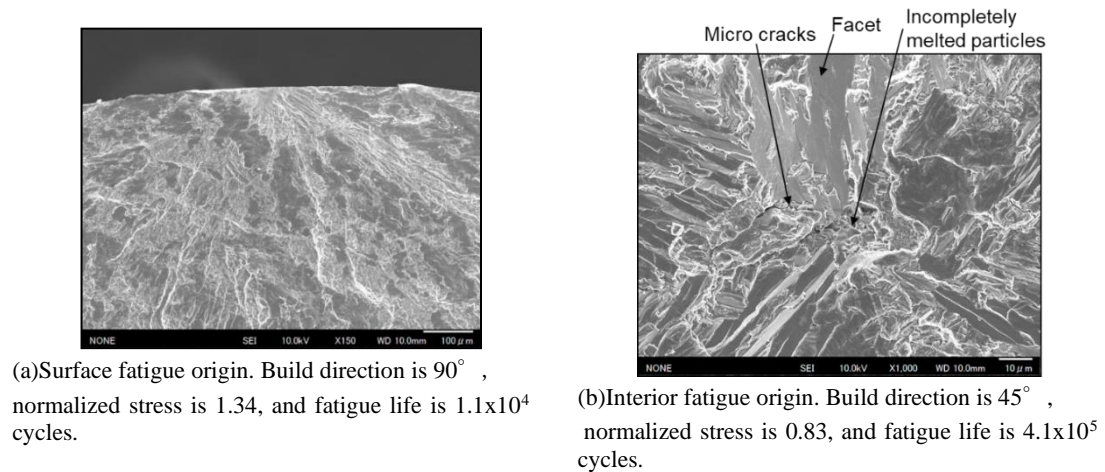


Figure 2.1-1 S-N diagram of EBM Ti-6Al-4V



(a) Surface fatigue origin. Build direction is 90° , normalized stress is 1.34, and fatigue life is 1.1x10⁴ cycles.

(b) Interior fatigue origin. Build direction is 45° , normalized stress is 0.83, and fatigue life is 4.1x10⁵ cycles.

Figure 2.1-2 Fractography of EBM Ti-6Al-4V

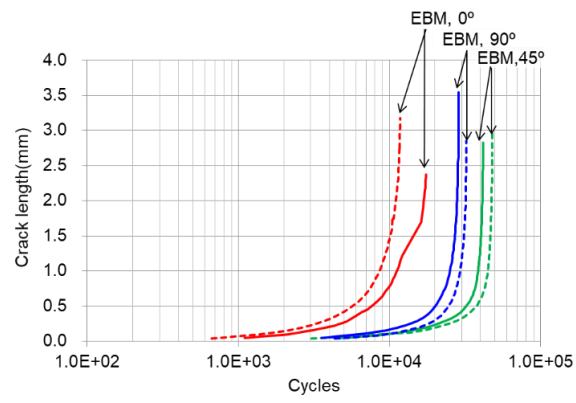


Figure 2.1-3 Crack length versus cycles of EBM Ti-6Al-4V with different build direction

3. FATIGUE AND FAILURE IN COMPOSITE MATERIALS AND COMPONENTS

3.1 Effect of Interface Nanostructure on Fatigue Delamination Growth of CFRTP and Aluminum Alloy Jointed by Direct Thermal Welding

Atsushi Hosoi^{1,2}, Kei Saito¹, Kristine Munk Jespersen^{1,3}, Hiroki Ota¹, Keita Wada¹, Hiroyuki Kawada^{1,2}

¹ Waseda University, Tokyo, Japan

² Kagami Memorial Research Institute for Material Science and Technology, Waseda University, Tokyo, Japan

³ Kanagawa Institute of Industrial Science and Technology (KISTEC), Kanagawa, Japan

With the recent demand for weight reduction, structural materials for transportation equipment are being replaced by carbon-fiber-reinforced thermoplastics (CFRTPs). Therefore, techniques to join CFRTPs to alloys are needed. In this study, the fatigue delamination growth of bonded CFRTP/aluminum alloy joints was characterized using double cantilever beam specimens, which consisted of plain woven CFRTP with PA6 as matrix and aluminum alloy (A5052). Three types of specimens bonded using different methods were tested; specimens bonded by adhesive (Adh), specimens directly bonded after silane coupling treatment (Si-AR), and specimens directly bonded after fabricating a nanostructure on the surface of aluminum with subsequent silane coupling treatment (Si-NS). Fatigue loading was applied in displacement control mode. The ratio between the minimum and maximum (displacement ratio) was 0.1, and the test frequency was 5 Hz. The crack length during the fatigue tests was obtained by compliance calibration. The nanostructure was fabricated by repeated anodizing and etching treatments. First, the aluminum alloy was degreased by acetone in an ultrasonic cleaner. Then, an initial anodizing treatment was performed for 9 h followed by a 60-min etching treatment. Subsequently, secondary anodizing and etching treatments were performed for 9 h and 20 min, respectively. The anodizing and etching processes were carried out at 10 °C and 63 °C, respectively. Figure 3.1-1 shows the aluminum surface for Si-NS, on which the nanostructure was fabricated. In the area where the crack propagated during the fatigue test, expanded porous shaped holes were present on the surface, with a diameter of approximately 0.32 μm and density of 5.3 pores/μm². Fatigue delamination growth was characterized by Paris diagram for each specimen type as shown in Fig. 3.1-2. The fracture surface distinctively changed from smooth brittle-like fracture to hair-like ductile fracture post fabricating a nanostructure and chemical bonding as shown in Fig. 3.1-3. As a result, the fatigue delamination growth resistance of the specimen with the nanostructure significantly improved due to the hair-like ductile fracture.

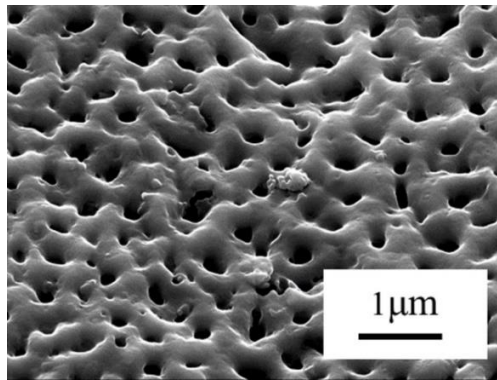


Figure 3.1-1 SEM images of on nanostructured aluminum surface

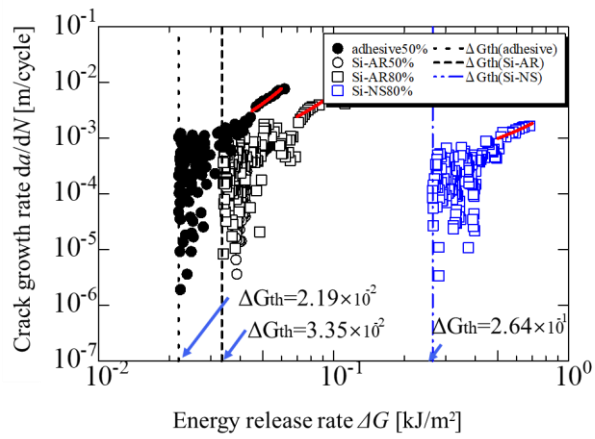


Figure 3.1-2 Paris diagram comparing the DCB fatigue test results of the Adh, Si-AR, and Si-NS

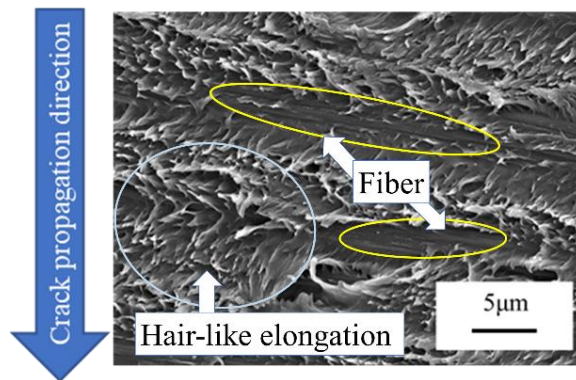


Figure 3.1-3 Fracture surface of CFRTP laminates bonded with aluminum alloy with nanostructure surface

3.2 Improving Damage Tolerance of Composite T-joints Using Interlocking-Fiber-Based Crack Arrester

Shu Minakuchi, Shinsaku Hisada, Nobuo Takeda

The University of Tokyo, Chiba, Japan

One of the difficulties in composite structural application is joining components. A T-joint is a critical component in aircraft structures that transfers loads between vertical and horizontal panels. A critical concern of T joints is that cracks easily occur in the deltoid even during manufacturing [1] and immediately propagate along the flange-skin interface (Figure 3.2-1 (a)). Therefore, introducing crack arrest features at the flange-skin interface is effective in improving the damage tolerance of T-joints. This study introduced interlocking fiber features in the cracking interface and suppressed crack propagation utilizing massive fiber bridging [2]. Figure 3.2-1 (b) shows the basic concept of the proposed approach. The arrester consists of 0° layers with carbon fibers oriented in the crack propagation direction and 90° layers with carbon fibers oriented in the orthogonal direction to the 0° layers. When a crack passes through the intersection of the 0° layers, the 0° layers bridge and suppress the crack opening (Figure 3.2-1 (b) A). In addition, the 0° layers are prevented from peeling off at the bonded interface with the adherend by the 90° layers bridging between the 0° layers (Figure 3.2-1 (b) B). Therefore, for crack propagation, breaking carbon fibers of either the 0° or 90° layers is necessary. This mechanism significantly improves the apparent fracture toughness and the energy absorption characteristics (Figure 3.2-1 (c) [2]).

Pull-up tests were conducted to verify the effectiveness of the interlocking-fiber-based crack arrester in composite T-joints [3]. Figure 3.2-2 compares the deformation of specimens without and with the arrester. In the case of the specimen without the arrester, the pull-up load decreased significantly due to crack generation at the interface of the deltoid and the corner of the L-shaped part. When the crack began to propagate along the deltoid-skin interface, the load decreased again. Finally, the crack propagated immediately at the flange-skin interface, leading to final failure. In contrast, in the specimen with the arrester, the crack propagation at the flange-skin interface was suppressed at the arrester places. Final failure occurred because of the fracture of the 0° layers of the arrester. Figure 3.2-3 compares the load–displacement curves of the eight specimens without and with the arrester. The specimens with the arrester showed much greater displacement than those without the arrester, confirming the effectiveness of the proposed arrester concept for improving the damage tolerance of composite T-joints.

[1] Hisada, S., Minakuchi, S., & Takeda, N. (2021). Cure-induced strain and failure in deltoid of composite T-joints. *Composites Part A: Applied Science and Manufacturing*, 141, 106210.

[2] Hisada, S., Minakuchi, S., & Takeda, N. (2020). Effect of interlocking fiber configuration on mode-I disbond arresting in composite bonded joints, SAMPE JOURNAL, 56(5), 6-15

[3] Hisada, S., Minakuchi, S., & Takeda, N. (2020). Damage tolerance improvement of composite T-joint under pull-up conditions using an interlocking-fiber-based crack arrester. Composite Structures, 253, 112792.

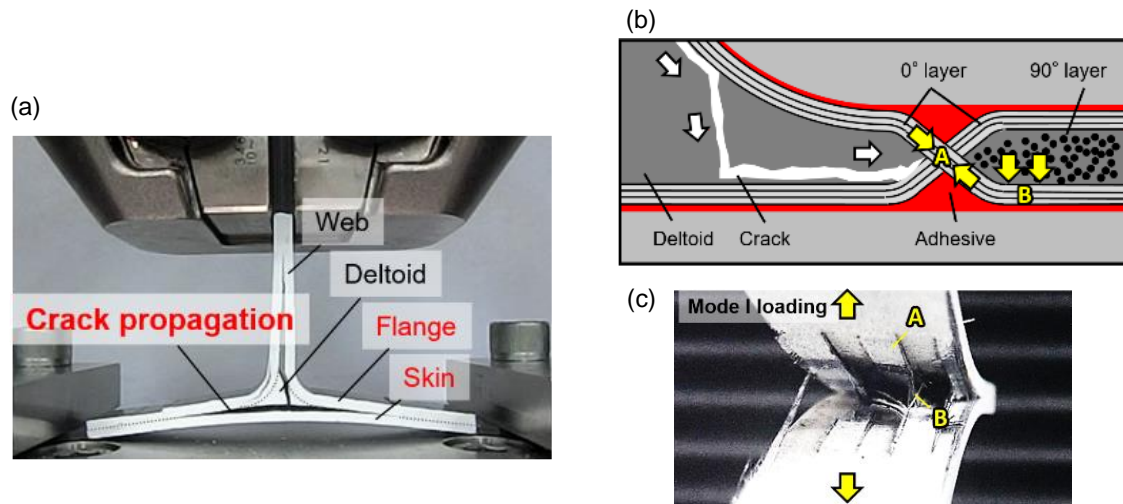


Figure 3.2-1 Schematic of interlocking-fiber-based crack arrester for composite T-joint. (a) Crack propagation along flange-skin bonded interface under pull-up condition. (b) Schematic of crack arresting. (c) Deformation and internal structure under Mode I loading

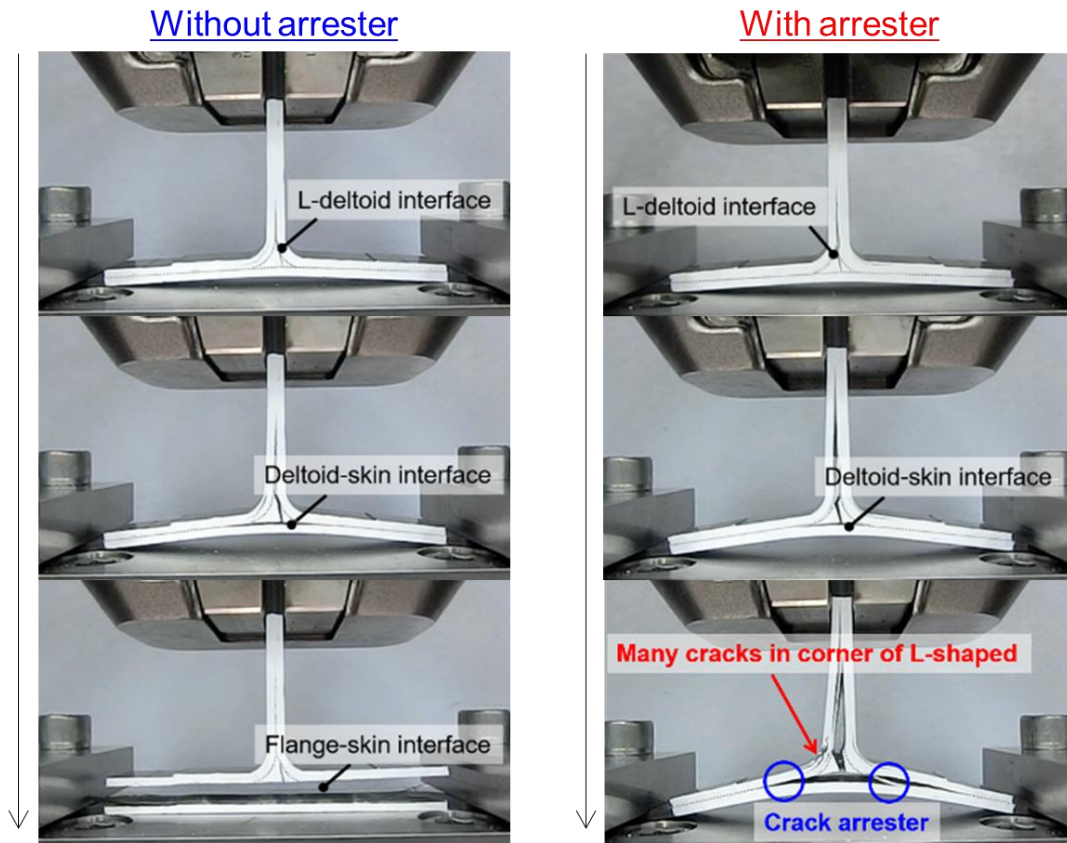


Figure 3.2-2 Deformation of specimens without and with the arrester

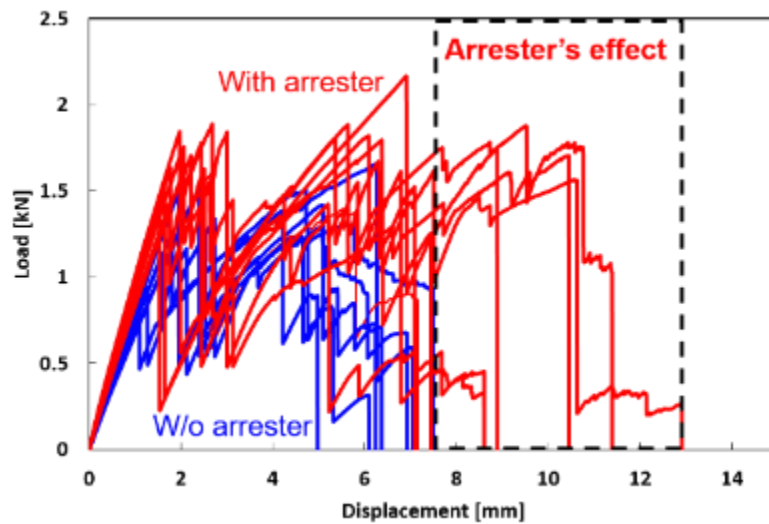


Figure 3.2-3 Comparison of load–displacement curves of specimens without and with arresters

3.3 Galvanic Corrosion Testing Procedures for CFRP-Metal Assemblies

Tetsuya Morimoto, Hisaya Katoh, Eiichi Hara and Yutaka Iwahori

Japan Aerospace Exploration Agency (JAXA), Tokyo, Japan

While corrosion has been an important cost factor in the maintenance, repair, and overhaul (MRO) of aircraft, specific strength has remained the primary consideration in the material selection in aircraft design. Consequently, only after entering operation does corrosion appear as a cost issue for current high-performance aircrafts.

CFRPs have been regarded as a potential material for application in the aerospace industry owing to their excellent specific strength and corrosion-free characteristic. The aerospace industry has been actively researching CFRP applications ranging from control surfaces and gear bay doors to, and more recently, larger components such as pressure bulkheads and stringer-frame structures. In addition, the use of CFRP combined with metallic components is expanding into other fields that deal with corrosive environments.

Corrosion risk for metals with CFRPs is rising as a new cost issue for newer generation aircrafts. This risk involves a drastically nobler galvanic potential than metals, and it develops during the formation of a global cell. For example, delivery of F-35s was suspended from September 21 to October 20, 2017 due to corrosion protection issues concerning the aluminum fasteners that fasten the CFRP external panels to the airframe.

Thus, galvanic corrosion in carbon fiber-reinforced plastic (CFRP) metal assemblies is a new and rising issue in aerospace structural design that is hindering the expansion of CFRP applications. The wide gap of galvanic potential between the metallic materials and the CFRPs causes an electrochemical reaction in the cell to occur that results in severe corrosion. Therefore, the evaluation of protection methods such as caulking, inhibitor painting, and water sealants using standardized procedures is essential. Present procedures such as ISO 9227 are intended for isolated samples. As such, galvanic paired samples of CFRP-metal assemblies are beyond their scope.

Therefore, the authors proposed the test standard which specifies the apparatus, reagents, and procedure to be used when conducting neutral salt spray (NSS), acetic acid salt spray (AASS), and copper-accelerated acetic acid salt spray (CASS) tests. And the authors evaluate the procedures through a series of galvanic corrosion tests for CFRP-Al bolted assemblies of Toray T800S/3900-2B composites and Al 1050P in direct contact with conductive bolts for three cases: no insulation, insulating film interface, and insulating film interface with insulated bolts. In the neutral salt spray (NSS) test, a 5% sodium chloride solution is atomized under a controlled environment. Figure 3.3-1 shows the schematic diagram of spray cabinet for galvanic corrosion tests. The chamber was controlled

for 100 h at 35 ± 1 °C and 95% RH, and was exposed to a 5.0 wt.%, 7.0 pH NaCl solution spray at a rate of 9.0×10^2 l/h. Pictures of test specimens, set up and NSS test are shown in Fig. 3.3-2.

As depicted in Fig. 3.3-3, A11050 shows a large weight loss accompanying galvanic corrosion in the conductive cases. This implies that any aluminum alloy, including corrosion resistant alclad, is corrosion sensitive in the assembled form with CFRP. As the application of CFRP-metal assemblies expands in the future, small scale corrosion, which has been neglected in the past, may become serious as larger scale galvanic corrosion becomes more frequent. Therefore, it is necessary to develop methods to suppress galvanic corrosion as well as standards to evaluate those methods.

In 2019, the proposed test procedures are adopted as ISO/CD 21746 standard galvanic corrosion testing procedures for CFRP-metal assemblies.

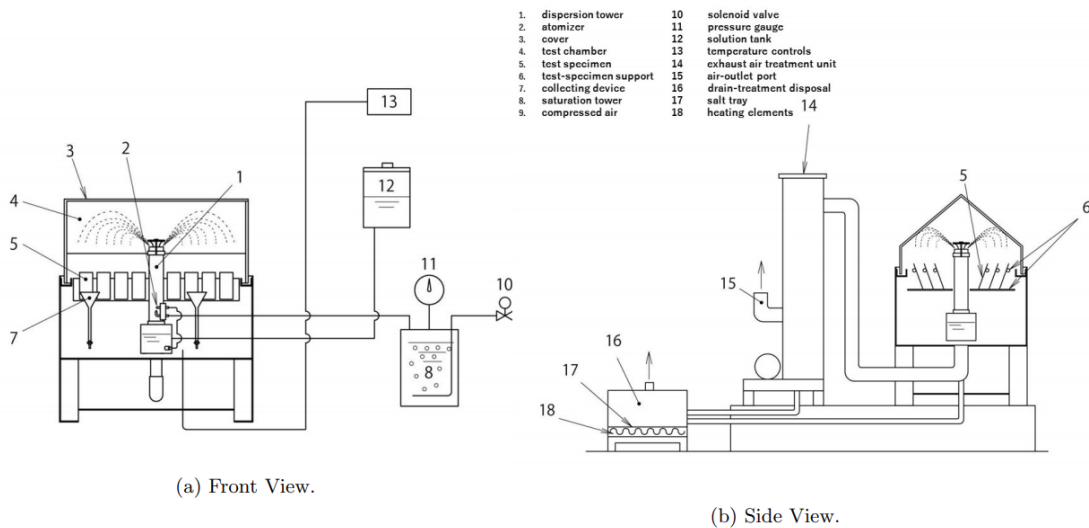


Figure 3.3-1 Schematic diagram of spray cabinet for galvanic corrosion tests

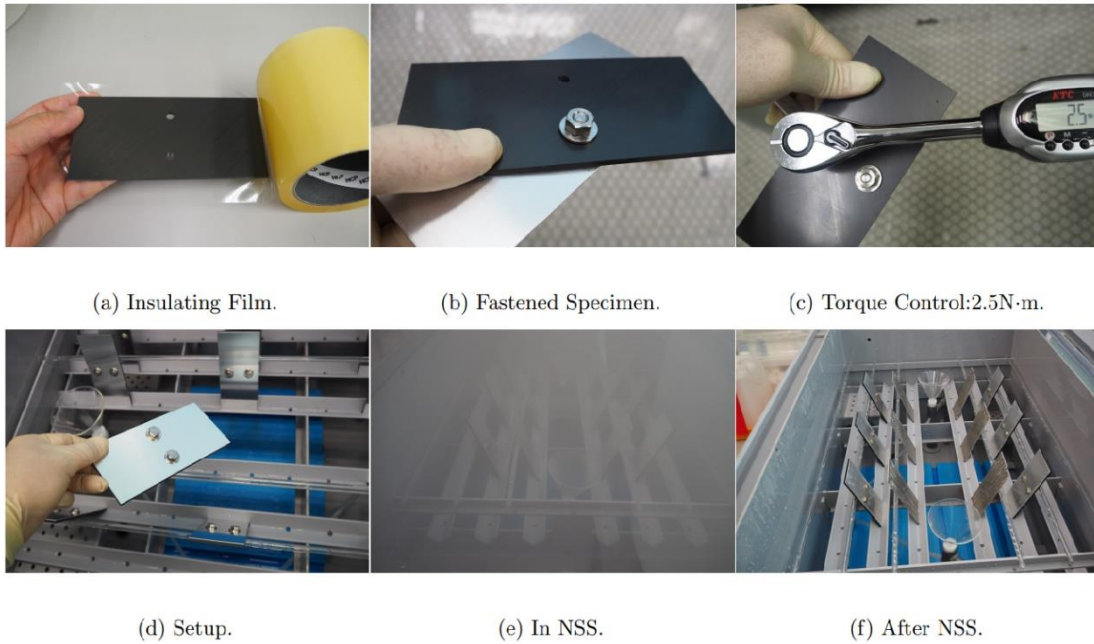


Figure 3.3-2 NSS tests for bolted CFRP-Al specimen

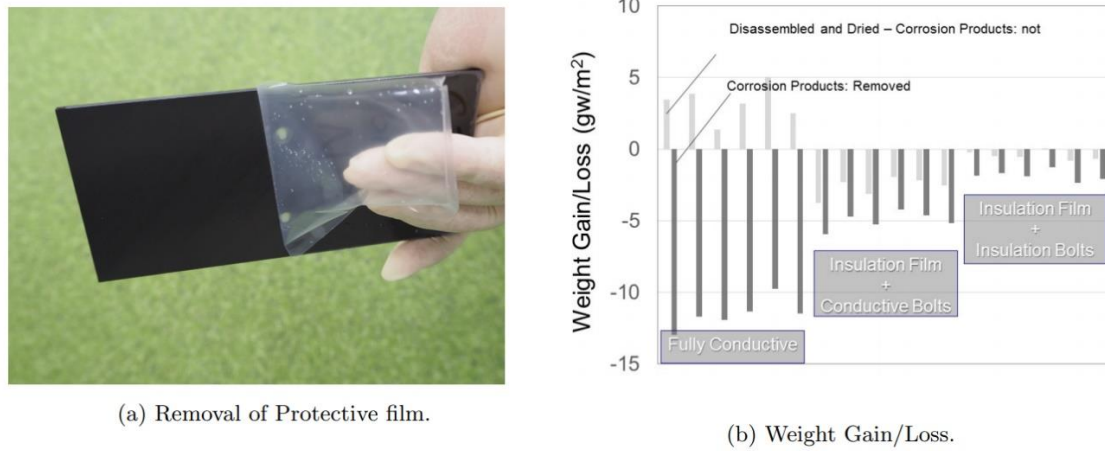


Figure 3.3-3 Weight Gain/Loss in NSS tests for bolted CFRP-Al specimen

3.4 Design and Manufacturing Trial of a Biomimetic Structure Based on Topology Optimization

Yuichiro Aoki, Kazushi Sasaki Toshiya Nakamura
 Japan Aerospace Exploration Agency (JAXA), Tokyo, Japan

In order to obtain an ideal lightweight design of the aircraft wing structure using CFRP (Carbon Fiber

Reinforced Plastics), a new airframe design method utilizing technologies in different field such as biomimetics has to be proposed and a topology optimization method is one of the candidate technique. Two types of load condition such as upward and downward bending are employed for the evaluation. The topology optimization method achieves the optimized structure, that is a layout of the reinforcement member, by decreasing the density of the structure based on the extent of the internal load. The deformation of the structure is minimized by the optimization. The volume of the structure and the maximum and minimum size of the element are set to the constraint condition. After topology optimization, the obtained reinforcement member is combined with the external skin and the size of the skin made by the CFRP is optimized to minimize the structural weight. The buckling load, allowable strain, thickness of the lamina, ratio of the ply angle, angle of the ply drop-off and etc. are set to the constraint condition. These two methods are employed repeatedly to reach the convergence of the structural weight.

By the proposed optimization, following results are obtained: 1) The reinforcement structure on upper and lower skin branches along span direction. This feature is different from the conventional wing structure. 2) On upper skin, the distance between reinforcement structures and its length are smaller comparing to those on the lower skin, because the upper skin has to sustain the buckling load.

Figure 3.4-1 compares the estimated wing weight. The weight is calculated from the FEM model of the wing structure. The weight of the wing structure optimized by the proposed method decreases 32% of the structural weight comparing to the conventional CFRP structure. The proposed layout of the reinforcement structure decreases the skin thickness and could sustain larger wing load.

Next, the lower part of the reinforced wing skin is made by the AFP (Automated Fiber Placement). Figure 3.4-2 shows the proposed reinforcement structure on lower skin and the area within two bays in the middle of the main wing is manufactured. The layout of the reinforcement member (fine line) is revised based on the minimum radius of the tow steering (1000mm in this case). The final layout of the reinforcement member for trial production is shown as the bold line. The stacking sequence of the skin is [45/90/-45/0]_{2s} and that of the reinforcement member adds the 0 plies (32 layers) to the skin. The detailed information is shown in figure 3.4-3. Toray P2362W-19U is used for the trial production. AFP parameters such as stacking speed, compaction force, tape tension and etc. for the panel and for the stringer are adjusted through the trial production. During the trial production, several manufacturing issues such as tow pull-up, gap between tows and tow bridging are extracted and some of them are improved by the adjustment of the AFP parameters.

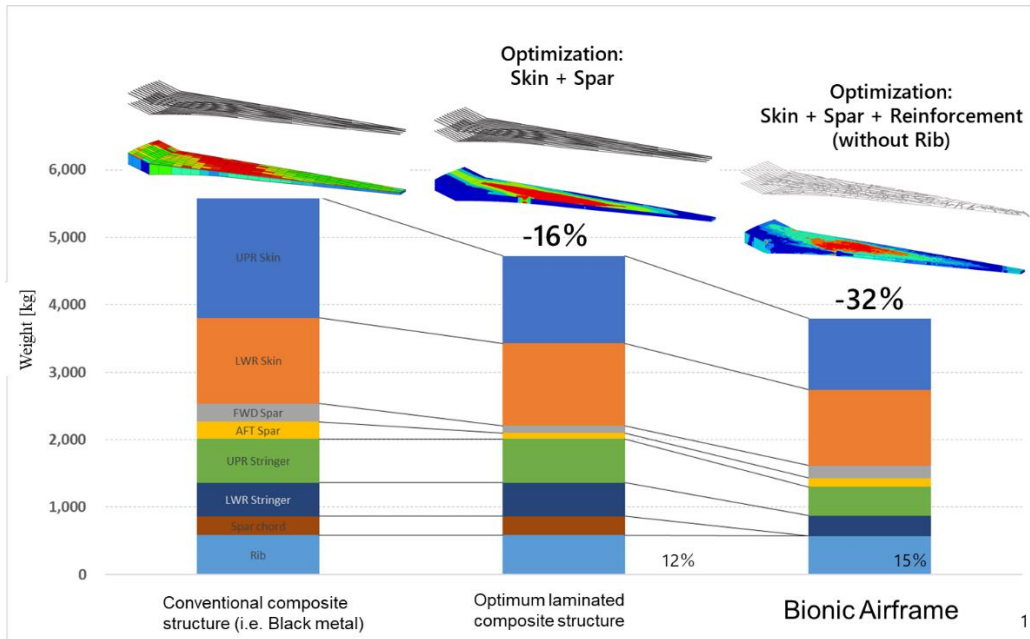


Figure 3.4-1 Comparison of the wing weight based on FEM model

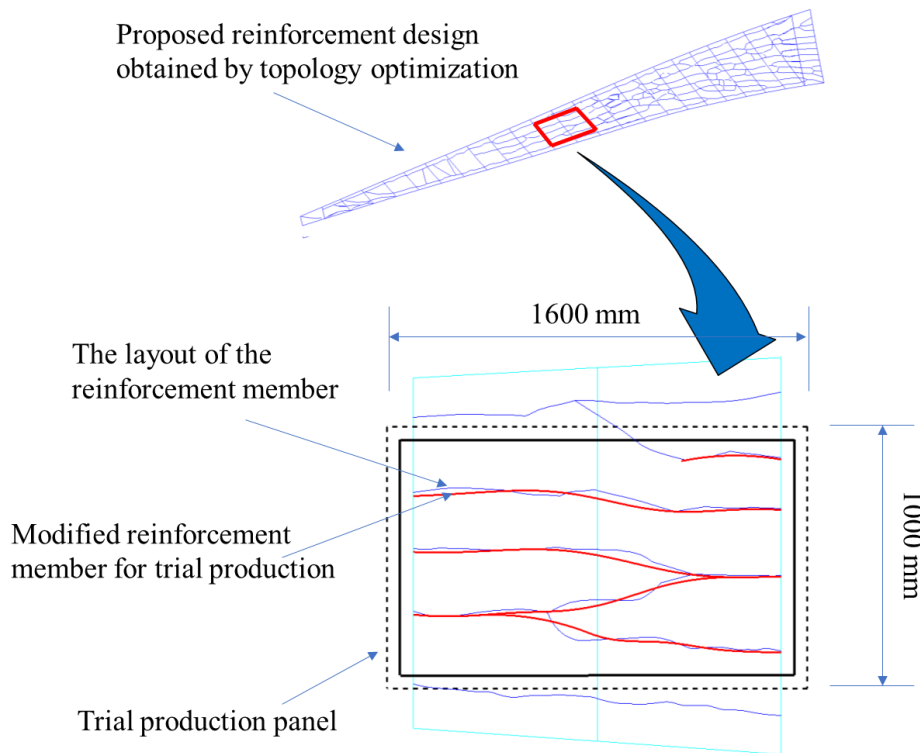


Figure 3.4-2 Schematic of the panel

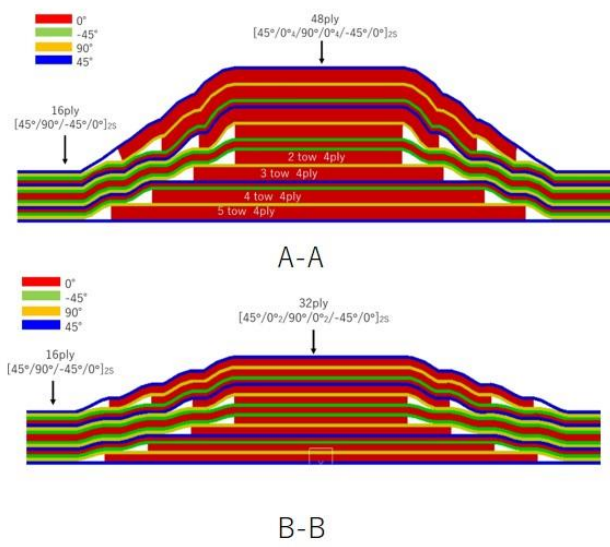
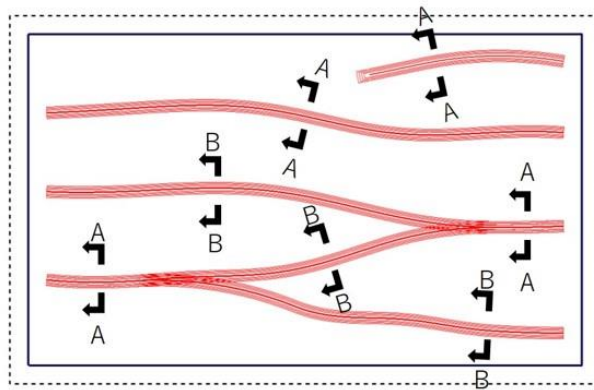


Figure 3.4-3 Stacking sequence

4 STRUCTURAL HEALTH MONITORING

4.1 Flight Demonstration Test for Optical Fiber Sensor based Impact Damage Detection System

Takuya Ishida¹, Yuji Ikeda¹, Kosaku Takahashi¹, Shu Minakuchi², Shin-ichi Takeda³, Noriyuki Sawai⁴

¹ Kawasaki Heavy Industries, Ltd., Gifu, Japan

² The University of Tokyo, Tokyo, Japan

³ Japan Aerospace Exploration Agency (JAXA), Tokyo, Japan

⁴ R&D Institute of Metals and Composites for Future Industries (RIMCOF), Tokyo, Japan

Kawasaki Heavy Industries, Ltd. (KHI) has developed a structural health monitoring (SHM) system capable of detecting impact damages using the optical fiber sensors namely Fiber Bragg Grating (FBG) sensors. FBG sensors are ideal for constructing a light-weight sensor network over a wide area of aircraft structures. The SHM system setup is shown in Figure 4.1-1. The FBG measurement unit is airworthy interrogator, which acquires strain data at ~800 kHz high-speed sampling in response to impacts. Simultaneously it acquires data with low-speed continuous sampling, for the purpose of load/usage monitoring. The objective of this development is to predict the best maintenance timing to minimize unexpected delays and opportunity loss of aircraft operations due to impact damage, etc.

Many types of system demonstration test have been performed in accordance with the building block approach. For example, sensor durability tests for various environment in coupon level, impact detection tests against various material impacts (steel, ice, concrete, rubber) in sub-structure level, and impact detection and durability demonstration in full-scale aircraft structure, as already reported at ICAF.

Further system demonstration in ground vibration test has been performed in 2018. In the random vibration environment according to RTCA DO-160G, the SHM system detected adequately small level impacts with a high probability, and without false call.

In 2019, flight demonstration test of SHM systems, in cooperative project with SUBARU CORPORATION and JAXA, has been conducted using JAXA's flying test bed "Hisho", Cessna 630. In this project, KHI has demonstrated the essential function of the SHM system. The sensor layout is shown in Figure 4.1-2. The sensor network with 4-FBG sensors was attached on a composite dummy panel, to substantiate that impact detection system works with sufficient reliability. And other FBG sensors were installed on the wing spar inside main-landing-gear well, to confirm that no false call occur in "Noisy" environment, that is the strain response of flight maneuvers, gear-up/down vibration, landing shock. The other FBG sensors were installed on the mid-fuselage crown stringer, to evaluate strain and temperature measurement accuracy, and to substantiate the simultaneous data record at low and high speed sampling.

362 times impacts by impact hammer were given to the dummy panel, and 356 times impacts were detected. POD curve was calculated and the detectable impact level was quantitatively evaluated (see Figure 4.1-3).

There was no false call. And low-speed continuous data were acquired simultaneously with high-speed impact detection data (see Figure 4.1-4). The data shows acceptable accuracy about strain and temperature. As a result of these works, “Practical” impact damage detection system has been demonstrated successfully.

This work was conducted under the contract from the New Energy and Industrial Technology Development Organization (NEDO), founded by the Ministry of Economy, Trade and Industry (METI) of Japan.

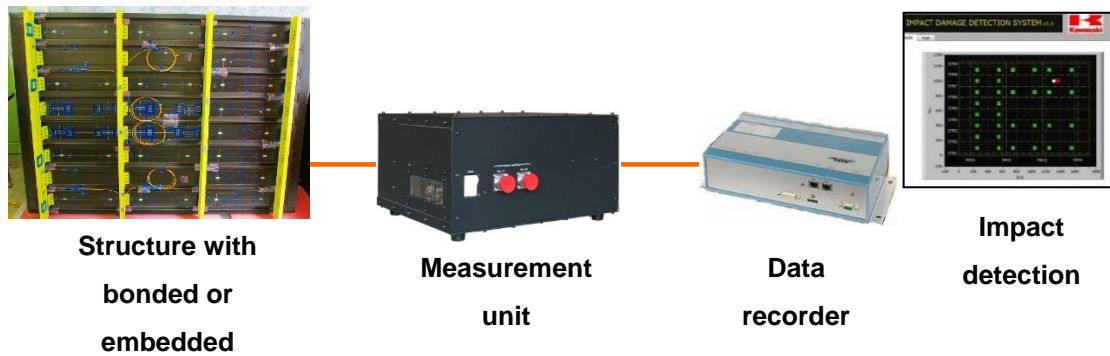


Figure 4.1-1 Impact damage detection system

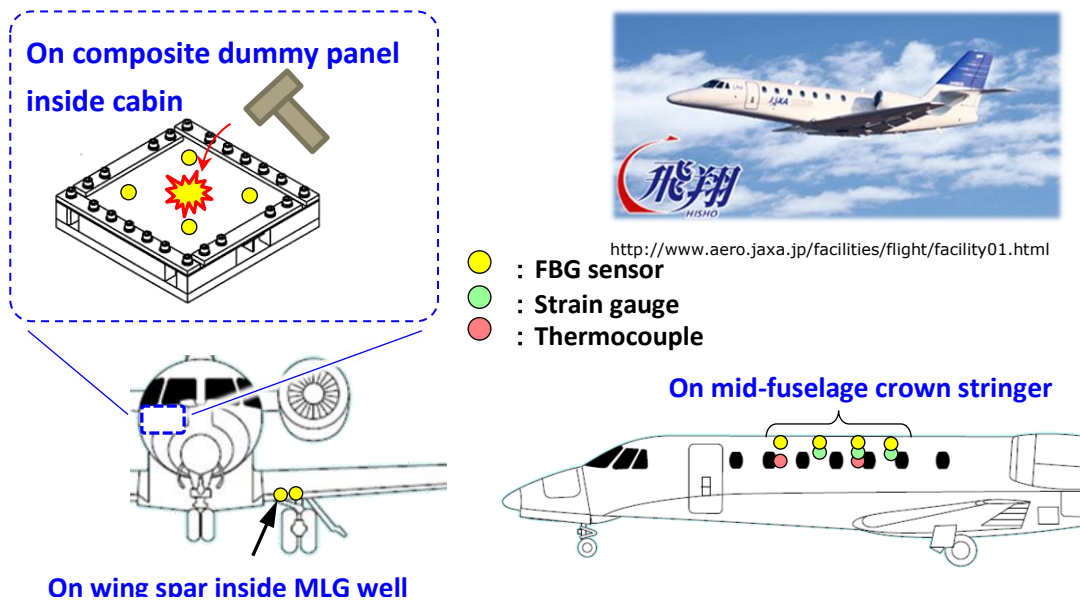


Figure 4.1-2 Sensor layout of flight demonstration test

<Hit / Miss Analysis>
by mh1823 POD software

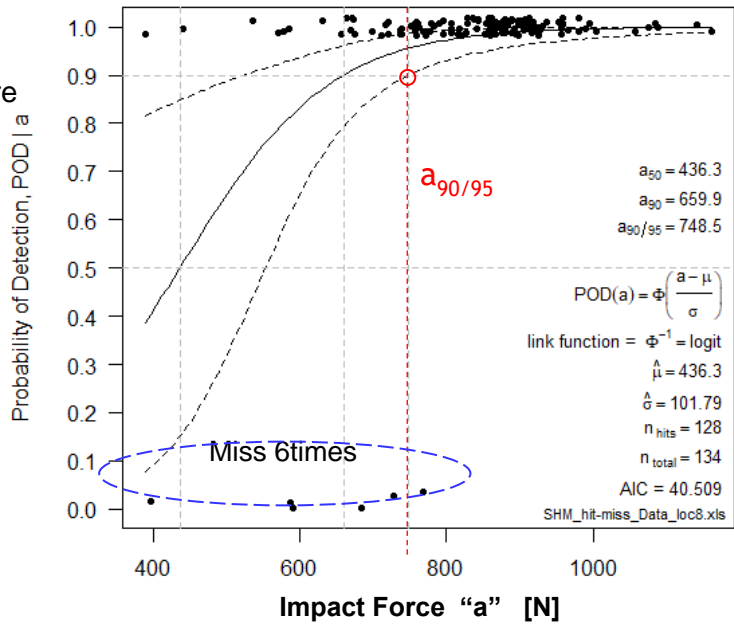


Figure 4.1-3 Example of POD curve acquired from flight demonstration test

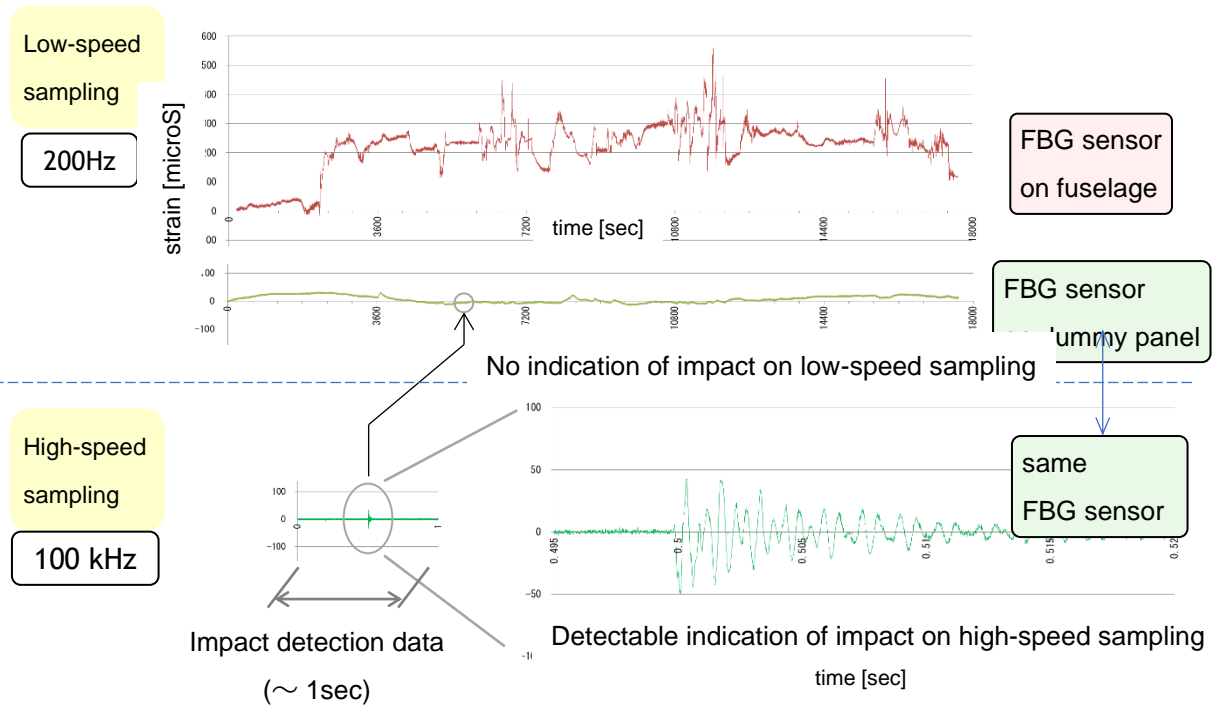


Figure 4.1-4 Simultaneous acquisition of low and high speed sampling data

5. MISCELLANEOUS

5.1 Smart Wing Load Alleviation Through Optical Fiber Sensing, Load Identification, and Deep Reinforcement Learning

Daichi Wada¹, Masato Tamayama¹ and Hideaki Murayama²

Japan Aerospace Exploration Agency (JAXA), Tokyo, Japan

The University of Tokyo, Tokyo, Japan

The use of optical fiber sensors has been considered to realize smart structures, which can sense and respond to different environments. Optical fiber sensing technique has been actively studied for application in aircraft structural monitoring. The low weight, thin form, immunity to electromagnetic fields, and distributed sensing capability of such sensors makes their installation minimally invasive while allowing the collection of spatially high-density data. Several researchers have monitored the wings of unmanned aerial vehicles (UAVs) by using multiplexed fiber Bragg gratings (FBGs), to investigate the time histories of the measured strains and wing deformations in flight. Passenger aircraft monitoring has also been realized by fully distributed sensing techniques. Specifically, a vertical tail, fuselage and main wings were monitored during flight, and a correlation between the strain distribution histories and aircraft maneuvers was observed. The fully distributed sensing realized observations and understandings of the overall structural responses of the wings and the fuselage to flight conditions.

To enhance the aircraft performance, it is necessary to reduce the loads on the aircraft. Reducing the loads experienced by an aircraft during operation can help reduce the structural weight, thereby improving the energy efficiency. To alleviate loads in a direct and adaptive manner, that is, to control loads in real time against a feedback of the actual applied loads, the actual loads must be monitored. It is not feasible to directly measure aerodynamic loads, because complex wing structures and weight limitations inhibit the installation of several pressure sensors and tubes. In this case, the loads can be estimated based on structural responses such as strains, although the obtained solutions may be unstable because the inverse problems to solve loads from strains tend to be ill-conditioned specifically when loads are distributed load. To obtain stable solutions, a neural-network-based approach has been studied and demonstrated the promising feasibility to identify the wing load distributions.

Recent advances in deep reinforcement learning techniques provide promising opportunities to realize load control. In such techniques, a reward function can be designed to reflect the desirable behavior, which could be multi-objective, such as alleviating wing moments while maintaining the lift loads. The controller learns to develop an optimum control law that can be as nonlinear as necessary to maximize the expected reward. Once trained, the neural network controllers output the optimum

actions for every state feedback without the need of iterative optimization, which helps in realizing real-time and adaptive control.

Considering this background, in this study, a load alleviation technique was developed by integrating optical fiber sensing, load identification, and deep-reinforcement-learning-based control technique in a closed-loop manner, to demonstrate the framework for a smart wing, which can sense, process, and respond adaptively.

Figure 5.1-1 shows the control diagram. Static load control was assumed, and a wing with multiple flaps and optical fiber sensors was developed. Multiplexed FBGs were used to enable effective and minimally invasive sensing of the distributed strains ϵ on the wing surface. Based on the sensing data and the flap angles d , the spanwise distributed wing loads \tilde{F} and angle of attack \tilde{a} were identified. To realize the state identification, a group of neural networks was employed. This group of neural networks were trained by supervised learning. The flaps were controlled by another neural network, whose inputs included the identified states \tilde{F} and \tilde{a} . This neural-network-based controller was trained through a deep reinforcement learning approach, in which the controller objective was to minimize the bending moment at the wing root $M = F \cdot x$, where x is the array of the distances from the wing root to the corresponding F elements. F elements represent the discrete loads corresponding to the out-of-plane wing load distribution along the wingspan. To maintain stable level flight while reducing the bending moment, the total lift load was required to be maintained at a constant value. For simplicity, it was assumed that the total out-of-plane wing load, which is a sum of the F elements remained constant. Consequently, the neural-network-based controller was trained considering the criteria of a higher reward corresponding to a larger moment alleviation $M_{ref} - M$ (when $M_{ref} > 0, M > 0$) and smaller load variation $|F_{ref} - F_{total}|$. Here, M_{ref} and F_{ref} denote the bending moment and total out-of-plane load at a reference state, respectively.

The wing schematic is shown in fig. 5.1-2. A high-aspect-ratio wing with multiple flaps was considered. The flaps were used to change the load distribution profiles along the wingspan. Fifteen and eight pressure ports were located on the upper and lower sides of each array, respectively. The out-of-plane components of the aerodynamic loads at eight individual flap sections were calculated by integrating the measured static pressures around the airfoil, and the out-of-plane loads were simply referred to as the wing loads.

The load distribution and angle of attack were key parameters to be input to the controller in real-time. These parameters were computed and identified from other observables, specifically, the optical fiber sensing data (60 data) and flap angles (8) employing a group of two neural networks. A deep reinforcement learning algorithm based on the deep Q-network (DQN) approach, which is a model-free and off-policy algorithm, was employed. The agent considered an action-value function $Q(s, a)$ to select an action to interact with the environment. The input state s consisted of the total load error

ΔF , load distribution F , flap angle d and angle of attack a . The output was a vector with 24 elements for the flaps shifts $\Delta\delta$, which could be interpreted as a 3×8 matrix of the action choices.

All the eight flaps performed a shift (or chose to remain still) simultaneously. The environment f_{env} emulated the wing load distribution F as an updated state.

The agent repeated the following steps: observe state s of the environment, select an action a to update the environment, and receive a reward r as a consequence. Using the Bellman equation, $Q(s, a)$ was iteratively targeted to be $r + \max_{a'} Q(s', a')$, in which s' and a' denote the state and the action in the next time step, respectively. To update $Q(s, a)$, the loss function L was defined as

$$L = \left(r + \gamma \max_{a'} Q(s', a') - Q(s, a) \right)^2$$

where $\gamma = 0.95$ is the discount factor. $Q(s, a)$ was updated in a supervised manner by using the Levenberg–Marquardt algorithm as an optimizer. The weights and biases were initialized using the Nguyen–Widrow initialization method. The learning parameters were derived from the previous study. The reward r was defined as

$$r = \begin{cases} -3n_\delta, & \text{if } 1.2M_{ref} - M < 0 \text{ or } |F_{ref} - \sum F| > 5N \\ (1.2M_{ref} - M) \left(1 - \left| \frac{F_{ref} - \sum F}{F_{ref}} \right| \right)^4 - 3n_\delta, & \text{otherwise} \end{cases}$$

The wind tunnel experiments demonstrated that the proposed approach could alleviate the static wing moment by 56.6% on average over the test duration from the initial state, and the total load variations could be maintained within a range of ± 5 N for 87.1% of the test duration.

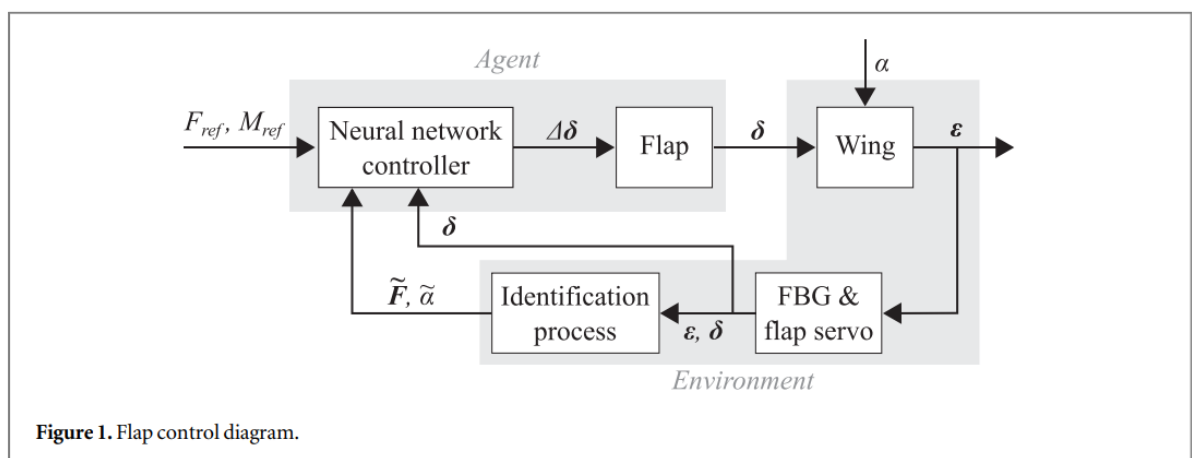


Figure 1. Flap control diagram.

Figure 5.1-1 Flap control diagram

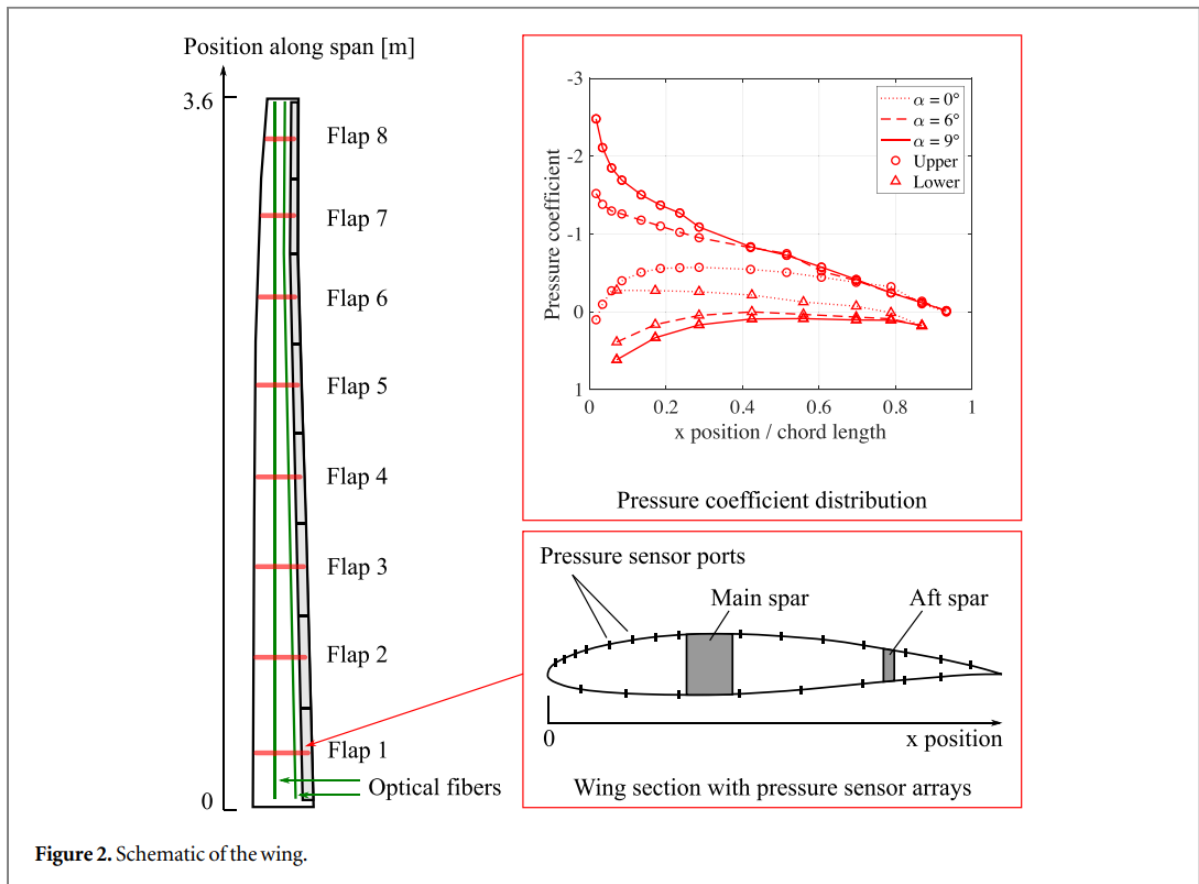


Figure 5.1-2 Schematic of wing

5.2 Scarf Sanding Technology for Carbon Fiber Reinforced Plastics (CFRP) Airframe

Hikaru Hoshi¹, Yuichiro Aoki¹, Eiichi Hara¹, Yutaka Iwahori¹, Yoshitaka Shiroyama², Hideyuki Shimizu², Eisuke Hoshiya², Katsumi Sugayama³ and Kazuhiko Sasaki²

¹ Japan Aerospace Exploration Agency (JAXA), Tokyo, Japan

² Shinmei Industry Co., Ltd. Aichi, Japan

³ Shinmei Tohoku Machinery Co., Ltd. Miyagi, Japan

Carbon fiber reinforced plastics (CFRP) have the advantage of being lighter in weight than metal materials, which is ideal for use in aircrafts' structural materials. With recent aircraft, the ratio of composites in the structural weight is increasing, with some containing 50 percent of the structural weight, and the number of aircraft applying composite airframe are expected to continue to increase due to the growing demand for further weight reduction. Aircraft are susceptible to damage from

lightning strikes, hail, stones that are kicked up from runway surfaces, tools that are accidentally dropped during routine maintenance and repairs, and so on. While such damage does not always affect the flight immediately, if cracks are left unattended, they could expand and cause severe accidents. For that reason, if small cracks of several centimeters are found on airframes, inspection and repair are conducted.

JAXA (Japan Aerospace Exploration Agency) has been engaged in research on automated scarf sanding technology to reduce labor and time burdens for the scarf sanding process of CFRP repair work. This is because the importance of CFRP repair technology is growing rapidly as the heavy maintenance of composite aircraft will begin in the 2020s. The standard method for CFRP repair work is shown in figure 5.2-1. First is to check the crack's width, depth and degree using NDT (Nondestructive Testing); next, the damaged area is sanded down into a mortar shape. Then, it is layered with repair materials and joined together with adhesive film. The work of scarf repair includes sanding down the damaged area into a conical shape. The scarf sanding process takes approximately 120 minutes for the technical expert working in facing downward position, and for novice technician, this work can take 480 minutes (300 minutes on average). If this scarf sanding process can be automated, anyone can perform the scarf sanding work without having expert technical skills in a short amount of time, as few as 100 minutes. Such automation can reduce the time required to do this work by 67 percent, and it is not always necessary to use people to do the work (Figure 5.2-2).

JAXA has been working with Shinmei Industry Co., Ltd., and Shinmei Tohoku Machinery Co., Ltd., to develop an Automated Scarf Sanding Device which applies JAXA's automated scarf sanding technology. The picture of the device is shown in figure. 5.2-3. This development is an outcome of the open innovation scheme named "JAXA Aeronautics Innovation Challenge 2016." The device is attached to the composite airframe with ten "legs" and conducts the scarf sanding automatically. The digital machining shape data entry and programming are not necessary to do this work. Now, we are improving the device's performance based on users' feedback, such as decreasing the weight of the device body (from 67 kg to 40 kg), reducing the amount of time required to perform the repair work, and increasing the durability of the cut and shaped area.

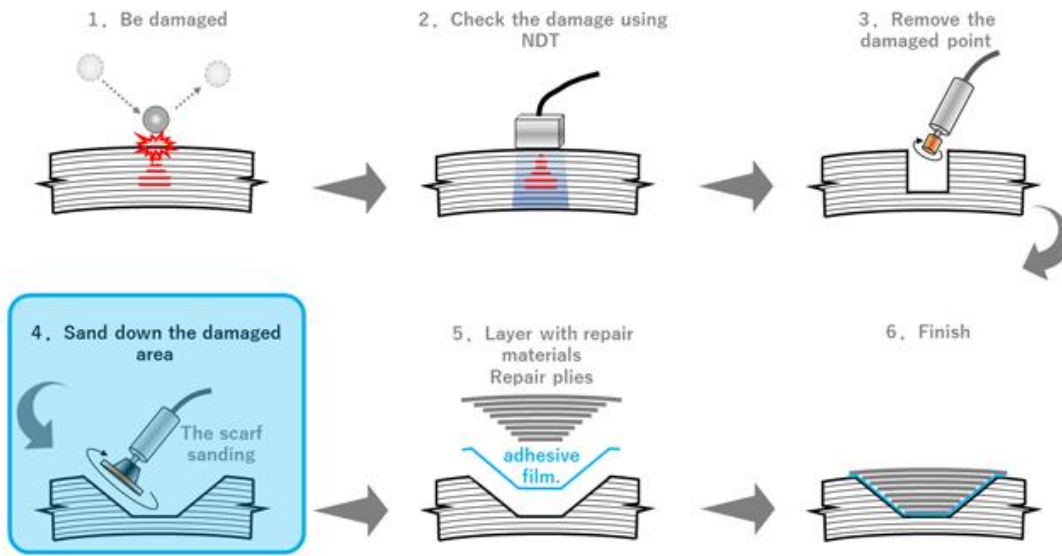


Figure 5.2-1 Scarf sanding method

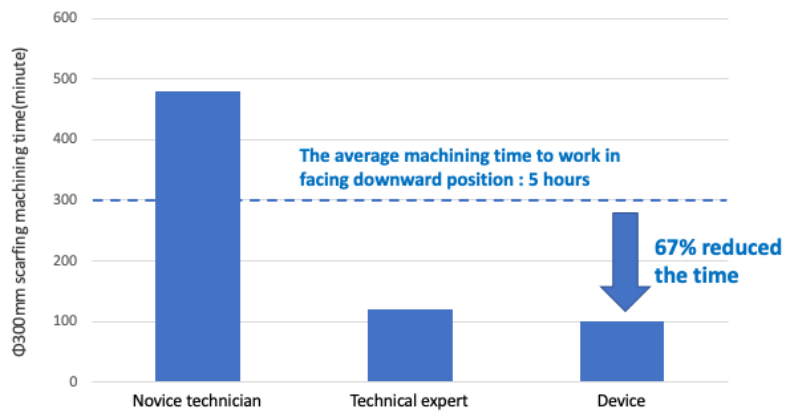


Figure 5.2-2 Comparison of machining time

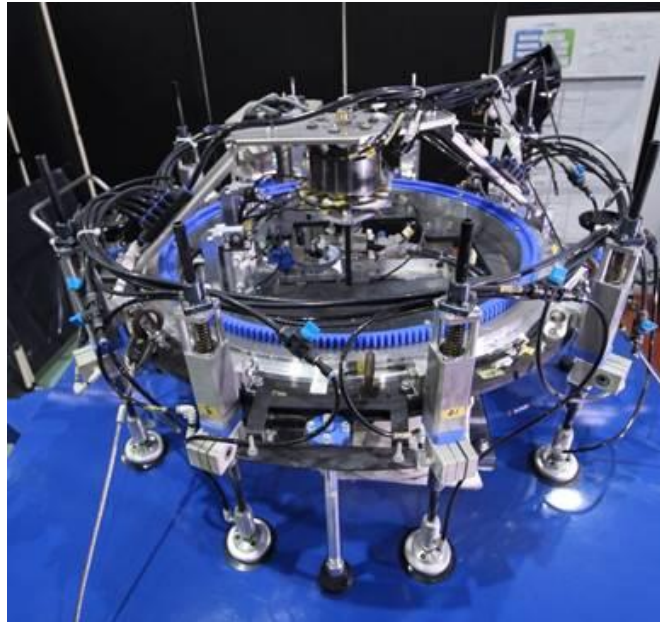


Figure 5.2-3 Photo of CFRP automated scarf sanding device

5.3 Measurement of the specimen surface by thermograph and DIC

Takao Okada

Japan Aerospace Exploration Agency (JAXA), Tokyo, Japan

The infrared measurement is currently used to measure the body temperature of the animals, to survey the leak of the gas from the pipeline, and to conduct the non-destructive investigation of the structure such as bridge and frame. Visualization of the extension of the airbag and ignite in the engine are also achieved by the infrared measurement. The stress (principal stress) measurement on the specimen during fatigue test is conducted using the lock-in technique. Emissivity (and appearance) on the surface will affect infrared emitted from the surface and the measured temperature using thermography may differ from the exact temperature on the surface, in case the surface has difference of the paint (No paint, Luster pain, Dull luster paint and etc.). Black dull luster paint is usually applied on the surface of the specimen before the test using thermography. On the other hand, DIC (Digital Image Correlation) has used in many engineering fields to measure the 2D and 3D deformation of the object in a decade. The speckle pattern is applied on the surface of the object to employ the DIC. The surface with speckle pattern causes non-uniform emissivity surface in general. Therefore, thermography and DIC could not be able to apply to the same surface. However, emissivity map, which is the distribution of the emissivity on the surface, might adjust the difference of the measured temperature on non-uniform emissivity surface and then might overcome the drawback.

In order to apply thermography to the specimen with non-uniform surface emissivity, evaluation to

develop the emissivity map of the specimen surface is conducted.

Toray prepreg T800S/3900-2B is used for the specimen and the stacking sequence of the specimen is [45/0/-45/90]s. The dimension of the specimen is 25mm wide, 235mm length and 1.67mm thick. The four types of the paint patterns are applied to the surface of the specimen in order to evaluate the difference of emissivity by paint pattern. The paint pattern is shown in figure 5.3-1. The thermography camera, FLIR ATS Co. SC7500, is used for the thermography measurement. The specimen is heated at 40 and 100 deg C in the environmental chamber and measure the temperature distribution using the thermography. The emissivity map is obtained using temperature distribution at these temperatures employing the software supplied by FLIR. Figure 5.3-2 shows the obtained result for stripe paint. By applying emissivity map, the difference of measured temperature caused by the difference of the emissivity is mitigated. Table 5.3-1 shows average temperature and the its span for each surface condition with and without applying the emissivity map. The result shows that the emissivity map is efficient for these paint condition.

Table 5.3-1 Measured temperature with and without emissivity map for each paint condition

	Emissivity map not adapted		Emissivity map adapted	
	Avg	Span	Avg	Span
Black	93.78	1.62	95.53	0.18
Stripe	93.08	2.74	95.62	0.24
Grid	93.46	3.21	95.70	0.44
Speckle	93.56	2.09	95.98	0.36

Paint pattern

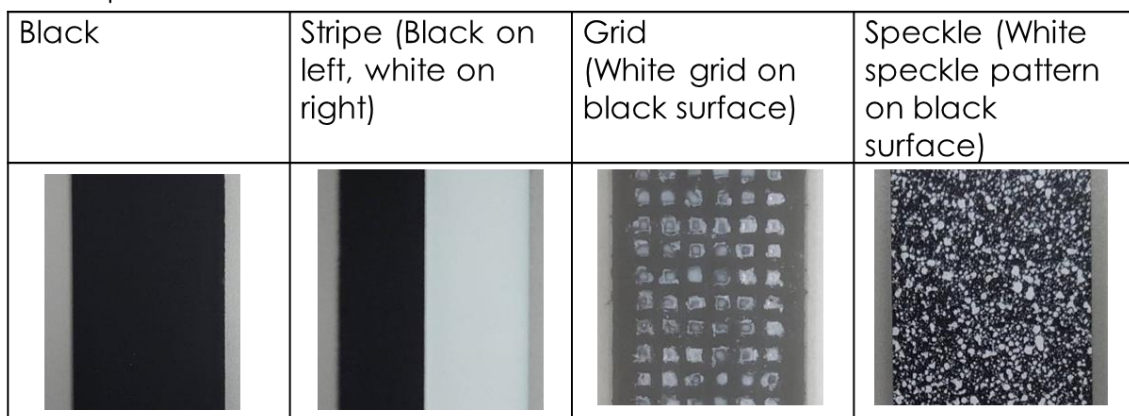


Figure 5.3-1 Paint pattern

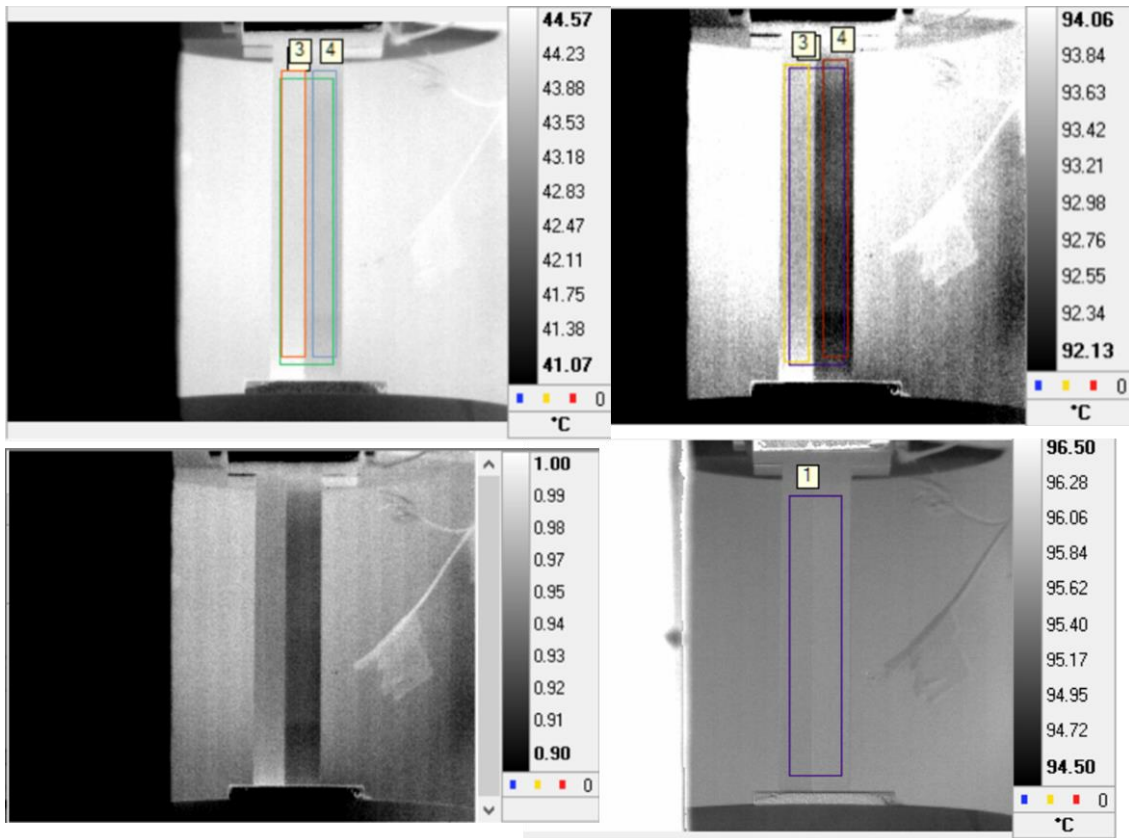


Figure 5.3-2 Temperature measurement result on stripe paint (a) 45 deg C, (b) 100 deg C, (c) emissivity map (d) 100 deg C with applying emissivity map

5.4 Aircraft Accident and Serious Incident Investigation

Yuji Yanagisawa

Japan Transport Safety Board (JTSB), Tokyo, Japan

(1) Total number of registered aircraft in Japan

As of December 31, 2020, the number of registered civil aircraft in Japan was 2,857, consisting of 1,366 airplanes (of which 660 airplanes are equipped with jet engines), 841 helicopters, 649 gliders inclusive of motor gliders, and one airship.

(2) Statistics related to the accident and serious incidents investigation

The number of accidents and serious incidents which JTSB investigated in the past two years are shown in Tables 5.4-1 and 5.4-2. Out of a total of 51 occurrences, large airplanes accidents and serious incidents were 22, small airplanes were 6 and rotorcraft were 10. Gliders, ULPs (ultra-light planes)

and others were remaining 13 occurrences.

(3) Fatigue failure related serious incident

1) Summary of the serious incident

On May 24, 2018, a Boeing 767-300 airplane experienced a failure of the left engine, while climbing after takeoff. The post-flight inspection revealed that HPT and LPT were damaged in several stages. Besides, the windows and roofs of the buildings and the windshield of cars on the ground were damaged by falling debris.

2) Damage to the Engine

The HPT Stage 2 blade in position #13 was fractured at the shank. The adjacent trailing blade was fractured at about midspan, and other downstream blades and stator vanes were also damaged, including a hole (crack) on LPT casing.

3) Metallurgical investigation of HPT Stage 2 blade #13

There existed two different areas on the fractured surface of the HPT Stage 2 blade #13, namely a smooth area (fatigue fracture area) and a rough area (rapid fracture area). In the smooth area, the fracture propagated from TA area where cooling air flow branches and turns around in the air passage 1 inside the blade. The beach mark indicating fatigue fracture was observed on the fracture surface in TA area (Figure 5.4-1).

4) Analysis of Findings

It is highly probable that the serious incident was caused by the fracture of HPT Stage 2 blade #13 of the left engine, due to cracks initiating from TA area of the blade.

The cracks in TA area were probably generated by low cycle fatigue initiating with the damage generated on the coating layer because the blisters were generated by hot corrosion and the cracks existed on the coating layer.

The cracks generated on the coating layer of the blade, which progressed to the base material and finally led to the blade fracture, were probably involved by a combination of multiple factors, namely increased cycles in service, steep rising shape of cooling air passage wall in the TA area (small curvature radius of TA area) and thickness of the coating layer.

Table 5.4-1 Number of Accident by Type of Aircraft

Aircraft Year	Large Airplane	Small Airplane	Rotorcraft	Glider, ULP or others	Total
2019	4	1	2	5	12
2020	4	1	3	5	13

Table 5.4-2 Number of Serious Incident by Type of Aircraft

Aircraft Year	Large Airplane	Small Airplane	Rotorcraft	Glider, ULP or others	Total
2019	10	3	2	2	17
2020	4	1	3	1	9

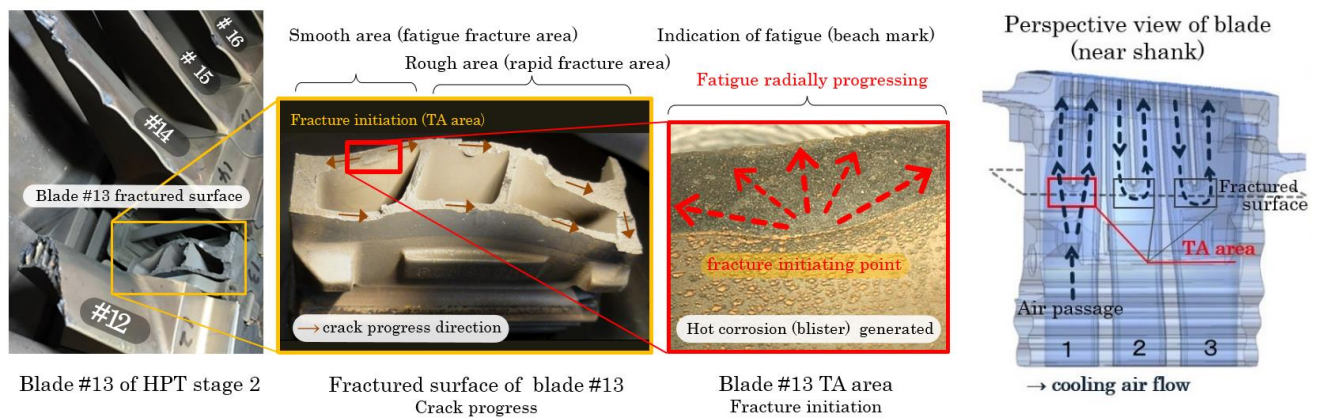


Figure 5.4-1 Fractured surface of HPT Stage 2 blade #13

ACKNOWLEDGEMENTS

The editors appreciated the members of the ICAF national committee of Japan Society for Aeronautical and Space Sciences and other participants in the committee, for their contribution in preparation of this national review and contributing discussion in the committee.